Achieving gradual failure under bending by the layering design of 3D printed continuous fiber reinforced composites

Tóth Cs., Vas L. M., Kovács N. K.

Results in Engineering 22 (2024) 102075

Contents lists available at ScienceDirect

Results in Engineering

journal homepage: www.sciencedirect.com/journal/results-in-engineering

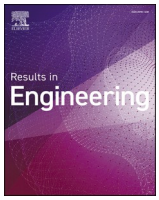

Achieving gradual failure under bending by the layering design of 3D printed continuous fiber reinforced composites

Csenge Tóth [a,b], László Mihály Vas [a], Norbert Krisztián Kovács [a,b,*]

[a] Department of Polymer Engineering, Faculty of Mechanical Engineering, Budapest University of Technology and Economics, Műegyetem rkp. 3., H-1111, Budapest, Hungary
[b] MTA-BME Lendület Lightweight Polymer Composites Research Group, Műegyetem rkp. 3., H-1111, Budapest, Hungary

ARTICLE INFO

Keywords:
3D printing
Continuous carbon fibers
Failure behavior
Four-point bending
Toughness

ABSTRACT

A variety of methods have emerged to tailor the mechanical properties of 3D-printed continuous fiber-reinforced thermoplastic composites (CFRTCs) through geometry design or manufacturing parameters. However, the potential to achieve customized failure behavior is not exploited. In this study, the effect of different layer orders on load bearing and failure of 3D-printed CFRTCs is investigated. Carbon fiber-reinforced polyamide composites with six layer orders were prepared and the mechanical response in 4-point bending was investigated. We show that the failure behavior ranges from catastrophic to pseudo-ductile, and we distinguished four typical stress-strain responses. We found that the location and the thickness of matrix-only layers strongly influence the failure. For the latter, we present a linear relationship to the ductility index which shows that toughness can be increased with thicker matrix layers. Our results facilitate the design of CFRTCs with customizable failure behavior, thus contributing to safer applications.

1. Introduction

There has been a second boom in material extrusion–based additive manufacturing technologies since the advent of continuous fiber composite methods [1]. Given the recent research efforts, the additive manufacturing of continuous fiber–reinforced thermoplastic composites (CFRTCs) is expected to have a notable part in the production of future structural components. The advantages of the technology are design flexibility, relatively low weight, and recyclability [2–4].

3D printed composites are multi-phase structures, in which beads (extruded filaments), lamina (one layer), and laminate (multiple layers) levels can be distinguished [5]. Voids are also regularly present at all levels [6–8]. As each level can be tailored, there are numerous design possibilities for 3D-printed composites. The fiber orientation, the fiber volume fraction [9], and even the fiber type can vary layer-by-layer [10] and stress-driven path planning algorithms are also emerging [11,12]. Due to the many design possibilities, and also the stochastic nature of defects [13,14], the response of 3D-printed CFRTCs to a given mechanical stress is not well predictable. Catastrophic failure is a major issue for composites [15–17], and it has also been experienced for 3D-printed CFRTCs [18]. Several different methods have been applied to overcome catastrophic failure. El Essawi et al. [19] studied the effects of manufacturing parameters and found the optimal settings to maximise tensile strength and energy absorption. Magyar et al. achieved increased ductility and gradual failure for epoxy-matrix carbon fiber-reinforced composites by using 3D-printed thermoplastic layers as adhesion modifier [20,21]. Huang and Joosten [22] prepared carbon/glass hybrids by 3D printing and reported their gradual failure process under tension. Vemuganti et al. [23] found that ductility can be increased by controlled fiber orientation, also under tensile load. Li et al. [24] found that the layer order design can delay delamination and failure. Fekete et al. [25] found that the failure modes are also altered by the addition of additives to the matrix material.

The design of the printed structure can also influence the failure mode under bending stress. Peng et al. [26] studied the energy absorption capacity and the failure behavior, and they found that crack propagation could be delayed by separating the fiber-reinforced layers. Their results were shown on continuous fiber-reinforced polyamide samples under 3-point bending. Dou et al. [27] prepared heterogeneous continuous carbon-fiber reinforced 3D-printed composites with different fiber volume fraction gradients and subjected them to 3-point bending load. The authors identified the main types of failure modes, namely:

* Corresponding author. Department of Polymer Engineering, Faculty of Mechanical Engineering, Budapest University of Technology and Economics, Műegyetem rkp. 3., H-1111, Budapest, Hungary.
E-mail address: kovacsn@pt.bme.hu (N.K. Kovács).

https://doi.org/10.1016/j.rineng.2024.102075
Received 5 December 2023; Received in revised form 18 March 2024; Accepted 27 March 2024
Available online 6 April 2024

surface fiber crush; fiber-matrix separation and fiber pullout caused by poor impregnation; fracture; interlayer separation caused by inadequate interlayer bonding. Zeng et al. [28] investigated the effects of manufacturing parameters (extruder temperature, printing speed, extrusion width and infill angle) on bending performance. They found that fiber pull-out is more likely to occur when the sample is prepared with higher printing speed, as the speed affects fiber-matrix bonding. Similarly, fiber pull-out was also observed with higher extrusion widths. As the extrusion width is reduced, the contact pressure increases, resulting in better fiber-matrix adhesion. Korkees et al. [29] investigated the effect of the position of the fiber-reinforced layers in the specimen on the bending properties. The authors identified tensile fracture of the outer layer and delamination as the main failure modes. Wan A Hamid et al. [30] found that under 3-point bending, 3D-printed continuous fiber-reinforced composites behave as a single structure until delamination occurs. Then, the composites can be considered as two individual beams. Their findings were supported by experimental tests and finite element simulations.

3D printing technology allows the preparation of corrugated structures by varying the infill density and the infill pattern. In this way, composite sandwich structures with a lattice core can be produced, which can have a positive effect when subjected to bending loads [31]. Li and Wang [32] showed that with different lattice geometries, different bending behavior can be achieved, and the failure mechanism can also be tailored. The truss core resulted in the highest flexural strength and stiffness, while the re-entrant honeycomb core increased the energy absorption capacity. Mat Daud et al. [33] showed that the energy absorption capacity can be further increased by introducing shear thickening fluids into the core. Zeng et al. [34] prepared failure maps for different corrugated sandwich structures fabricated with poly (lactic acid) matrix and continuous carbon fiber reinforcement. They revealed the failure mechanisms (face buckling, face yielding, core buckling and core yielding) as a function of the geometric parameters of the corrugated core. Pan et al. [35] investigated the flexural damage behavior, using micro-CT and acoustic emission technology. They prepared 3D-printed composites with continuous fiber-reinforced top and bottom layers and a triangular core with relative low infill density (37 %). The dominant damage modes were delamination and matrix buckling, and fiber fracture was also present when subjected to 3-point bending tests. Glass and Kevlar fibers were used as reinforcement and short carbon-fiber reinforced polyamide was used as matrix. In contrast, Maqsood and Rimasauskas [36] investigated continuous carbon fiber-reinforced poly (lactic acid) composites and found that the main damage modes were fiber breakage and pull-out under 3-point bending.

Overall, a growing number of methods have recently emerged to control the mechanical properties of 3D printed composites through layup design, or the printing parameters. However, achieving tailorable failure behavior is not being exploited. In addition, bending is frequently encountered in applications, but most studies focus on tensile load. In this paper, we investigate the effects of different layer orders on the load bearing and the failure behavior of 3D-printed CFRTCs, under bending load. Carbon fiber-reinforced unidirectional (UD) composites were prepared with different layer orders and two fiber volume fractions, and their mechanical response was monitored during 4-point bending tests. We identified the main damage modes, and we established a relationship between the failure process and the thickness of the unreinforced (matrix-only) layers. Our results provide new insights into the failure process of 3D printed composites and contribute to the safer application of these structures.

2. Materials and methods

2.1. Sample preparation and microstructure analysis

First, we designed four types of layer orders and investigated their response to bending. Two different types of layers were used: reinforced, and matrix-only (Fig. 1/b). The reinforced layers consist of PA matrix and carbon fibers, with the fibers laid in a concentric pattern (along the sides). Consequently, the fiber orientation remains parallel to the length of the specimen, resulting in quasi-unidirectional composites for all cases. There are also fibers perpendicular to the length at the ends of the specimens, but this is beyond the support and does not affect the measurement. Three fiber loops were laid in one layer, resulting in a 60 % fiber content. The matrix-only layers contain PA only, printed with a linear toolpath at 45° orientation (100 % infill density).

The fiber content and the specimen geometry were fixed (the geometry is shown in Fig. 1/a). The layer orders have been designed to progress from the most homogeneous (alt. 1) to the most heterogeneous possible (Top/bottom). Thus, the following four types were produced: alt. 1, alt. 3, alt. 5, and Top/bottom (Fig. 1/c) with 26.3 % fiber content. Based on the experimental results, we tested two additional layer orders with 15.0 % fiber content. With this reduced fiber content, we investigated the most homogeneous (alt. 1*) and the most heterogeneous (Top/bottom*) arrangements possible, which can be seen in Fig. 1/c.

All samples were manufactured with the Mark Two 3D printer from Markforged (USA). This system uses two nozzles, one for the PA matrix only, and one for the continuous fibers, which are also coated with PA. The nozzle temperature was 275 °C. We used solid infill pattern with 100 % infill density for the PA matrix. The layer height was 0.125 mm for the PA matrix only and the reinforced layers both. 1 wall contour was applied with a fixed thickness of 0.4 mm. Preparation of the 3D models for printing was done in the company's slicing software called Eiger. The specimens were produced with the NylonWhite type neat PA matrix supplied by Markforged with a diameter of 1.75 mm. The filament was stored in a drybox during printing to minimise moisture absorption. As reinforcement, a continuous carbon fiber filament was chosen also supplied by Markforged with a diameter of 350 μm. The carbon fiber filament consists of ~1000 single fibers [37]. According to the manufacturer, the tensile strength and tensile modulus of the continuous carbon fiber filament are 800 MPa and 60 GPa, and the flexural strength and flexural modulus are 540 MPa and 51 GPa, respectively. The tensile stress at yield and the tensile modulus of the PA matrix are 51 MPa and 1.7 GPa, respectively, and the flexural strength and flexural modulus are 50 MPa and 1.4 GPa, respectively [38].

To analyze porosity, we cut the samples, embedded them in epoxy, then polished the cross-sections using a Labopol-5 polishing machine from Struers (Denmark). Images were taken with a VHX-5000 optical microscope from Keyence (Japan) at eighty times magnification. The void area was determined by color segmentation using ImageJ software.

We also took Scanning Electron Microscope (SEM) images of the fracture surfaces. The samples were sputtered with gold to avoid static charging. The images were made with a JSM 6380LA scanning electron microscope from Jeol Ltd. (Japan).

2.2. Flexural properties

4-point bending tests were carried out on five specimens of each type on a Zwick Z020 universal testing machine (Germany) according to EN ISO 14125. In 4-point bending, the bending moment is constant between the upper compression heads and no out-of-plane shear occurs, so the loading is pure bending. In contrast, during 3-point bending, the bending moment increases towards the loading nose, resulting in increased shear and a concentrated force at the head that can cause the top layers to crack [39]. The cross-head speed was 10 mm/min. Fig. 2 shows the testing arrangement. The support span (L_s) is 66 mm, and the thickness (h) is 4 mm. Flexural strength (σ_f) is calculated based on EN ISO 14125 with Eq. (1).

$$\sigma_f = \frac{FL_s}{wh^2} \tag{1}$$

Where F (N) is the load, L_s (mm) is the span, w (mm) is the width of the

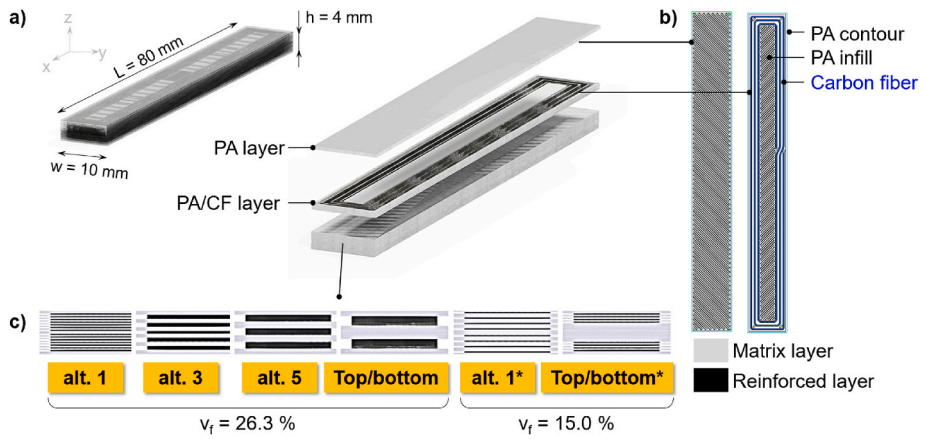

Fig. 1. Specimen properties: a) geometry and dimensions, b) layer types, c) schematics and description of the layer sequences.

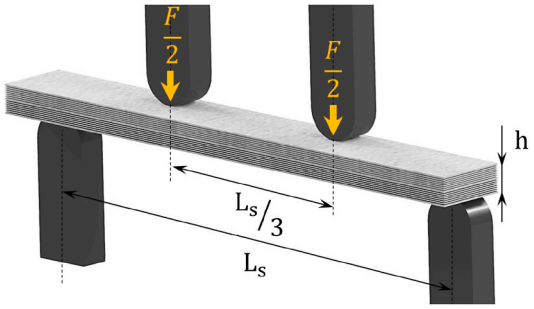

Fig. 2. 4-point bending arrangement (L_s = 66 mm, h = 4 mm).

specimen, and h (mm) is the height of the sample.

The area under the flexural curves correlates with the absorbed energy, therefore it can be used to determine the ductility index [40]. The amount of energy absorbed until maximum stress is the crack initiation energy (E_{CI}), and the rest is the crack propagation energy (E_{CP}). Total absorbed energy (E_T) is given as the sum of E_{CI} and E_{CP}. The ductility index (DI) can be calculated with Eq. (2) [20].

$$DI = E_{CI}/E_T \tag{2}$$

3. Results and discussion

3.1. Bending test results

We investigated the stress-strain curves and made video recordings of the samples during the tests (Fig. 3). The highest strength and modulus were measured for the Top/bottom type, in which the reinforcement is placed where the maximum stress is expected. For the other three types with 26 % fiber content, the differences in the flexural properties are small (the flexural modulus ranges from 16.4 to 16.9 GPa, and the flexural strength is between 238 and 254 MPa). In the case of the Top/bottom* type (15 % fiber content), the strength decreased to a maximum of 173 MPa, and the modulus decreased to a maximum of 12.4 GPa.

However, the layer orders showed differences in their failure behavior. For the alt. 1 and alt. 3 types, the failure is preceded by a non-linear curve phase, indicating a pseudo-ductile failure mode. For the alt. 1, failure was immediate, with no visible signs of damage (Fig. 3/a). The SEM image of the cross-section (Fig. 4/a) shows that damage modes are different in the upper and lower parts of the specimen. In the compressed zone (upper) fibers broke (Fig. 4/b), and toward the tensile region (lower) delamination increased (Fig. 4/c). In case of the samples with lower fiber content (alt.1* type), delamination was observed in the upper half of the specimens. Complete failure was preceded by the breakage of the bottom layers. In the case of the alt. 3 specimens, Fig. 3/b shows a small buckling at the top side, where the specimen is compressed, right before the samples break. The SEM image (Fig. 4/d) showed that the compression caused the top fiber layer to buckle up and separate from the matrix layers. In the case of the lower fibrous layer, the fiber bundles were pulled out together by the tensile force. The matrix layers also showed brittle fractures. The failure process of the alt. 5 type was multi-stage. It also showed non-linear (quasi-ductile) sections before failure. Fiber buckling was detected as the reinforced group of layers broke at the top (Fig. 3/c). After that, the samples either failed catastrophically or broke in two stages. The SEM image of the cross-section (Fig. 4/f) revealed a transition in failure mode from the upper half to the lower half. In the top fibrous layer, fiber breakage was dominant (Fig. 4/g); in the middle, a mixed failure mode with fiber breakage and pull-out was observed. The fiber pull-out may be visible because the composite did not break along a single plane, the fiber break occurred at a point in the layer that is not visible and then pulled out. The lower reinforced layers showed fiber pull-out and delamination. It can also be seen that occasionally the elementary matrix filaments separate from each other, indicating inadequate polymer bonding. The failure behavior of the Top/bottom type can also be divided into separate steps. The upper group of fibers broke first, with visible buckling (Fig. 3/d). However, complete failure was delayed. As the upper fibers broke, the elongation of the PA core was not inhibited any longer, and a plateau-like section appeared on the curves. The tests ended with the failure of the bottom fibers. In case of lower fiber content (Top/bottom* type) the buckling and delamination of the top fiber layers were more prominent, which can be due to adhesion between the layers. The SEM images in Fig. 4/h-i show that the upper fiber layers have been disrupted by clean breakage. In the lower half, the fiber bundles separated from the matrix, and the fibers slipped out (Fig. 4/j). Clear separation can be seen between the filaments and the surrounding matrix. This gradual failure process has resulted in a delay of the complete fracture and a rise in elongation. Similar damage modes were reported by Li et al. [41] for 3-point bending, where fiber breakage was identified in the compressive region, and fiber pull-out in the tensile region. Pan et al. [35] also reported debonding and delamination in the upper and lower layers during flexural failure of 3D printed continuous fiber-reinforced composites.

Based on the experimental results we can conclude that the layer order design greatly affects the failure behavior. The differences can also be seen in Fig. 5/a, where a representative stress-strain curve from each type was plotted. We also calculated the ductility indices (DI) for all layer orders and plotted them against the maximum thickness of the matrix-only layers in a sample (w_{matrix}) (Fig. 5/b). The DI is a dimensionless parameter between 0 and 1, where 1 means completely brittle

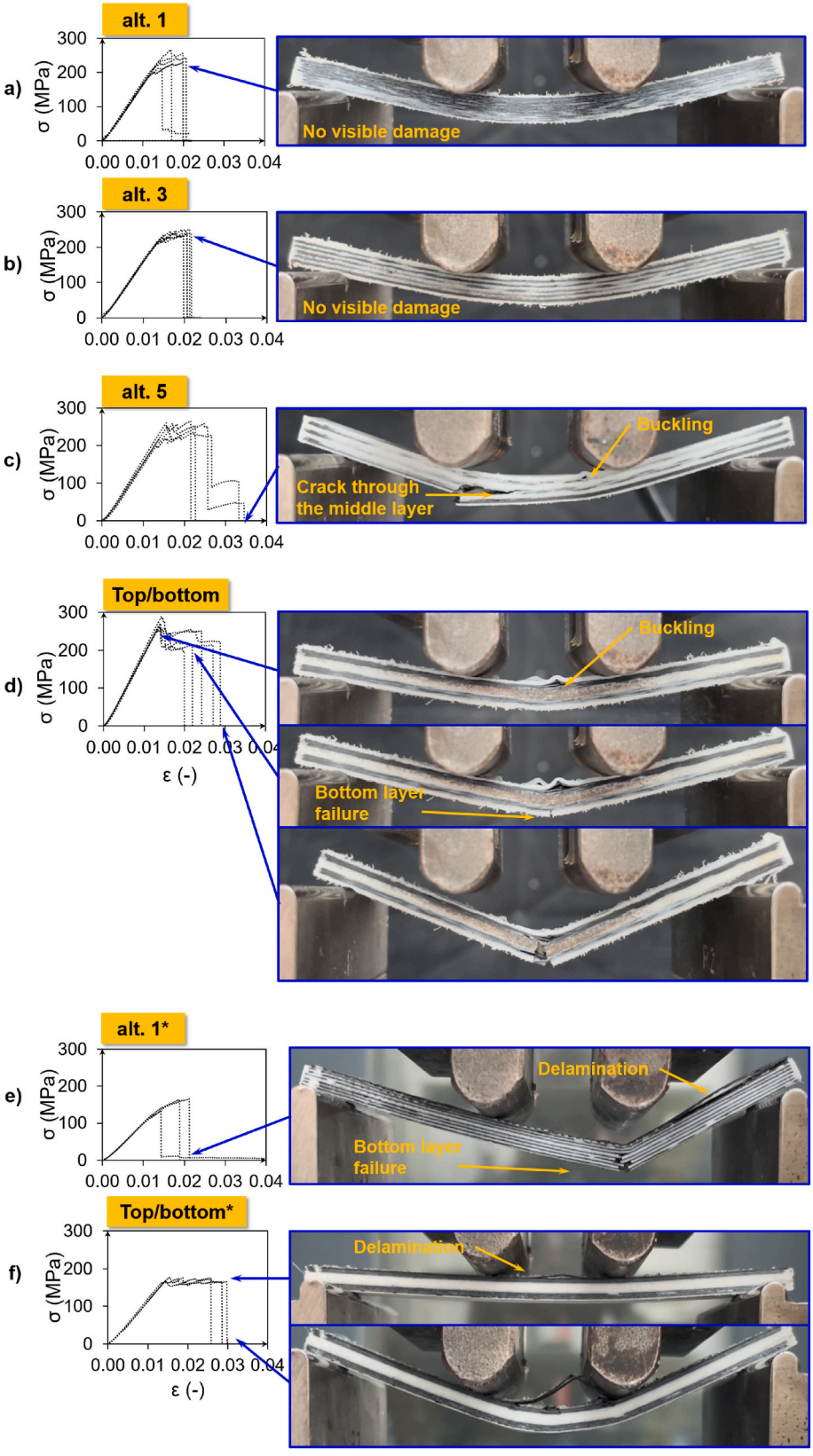

Fig. 3. Flexural stress–strain curves and images of the specimens during the tests for 26 % fiber content a) alt. 1, b) alt. 3, c) alt. 5, d) Top/bottom, and for 15 % fiber content e) alt. 1*, f) Top/bottom*.

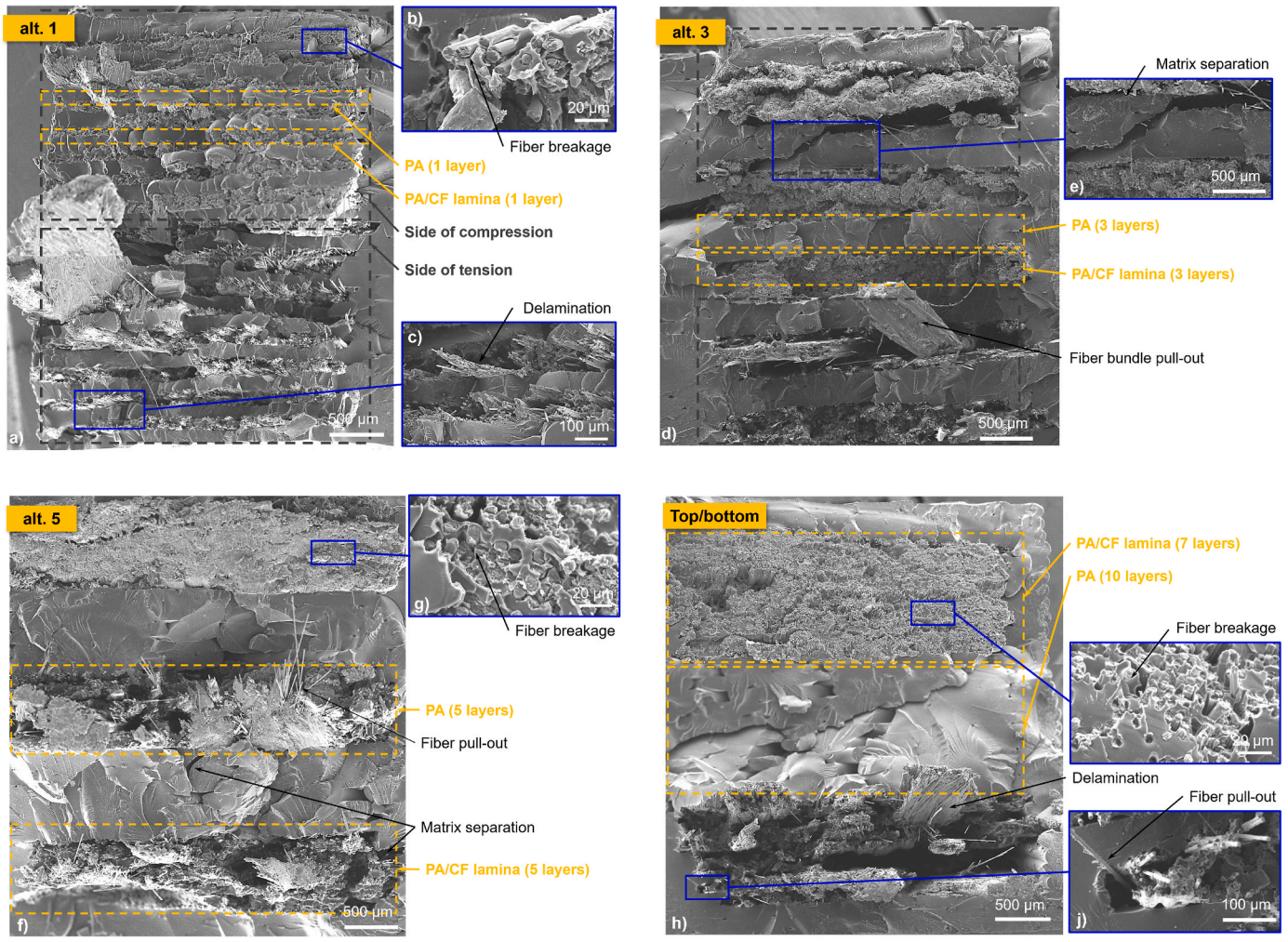

Fig. 4. SEM images of the fracture surfaces in case of the a) alt. 1, d) alt. 3, f) alt. 5, and h) Top/bottom types; signs of fiber breakage are shown on b), g) and i); c) shows signs of delamination, e) shows the matrix crack and j) shows fiber-matrix debonding.

behavior. As the thickness of the matrix layers increases, the DI decreases, which means the composites exhibit tougher behavior. We found that the linear relationship between DI and w_{matrix} is given by Eq. (3) ($R^2 = 0.9873$). With more PA-only layers between the reinforced ones, more reinforcement was placed in the heavily loaded parts of the test specimens (tension and compression side), therefore the flexural strength also increased. These findings apply to both fiber contents. In general, the two extremes of the layer orders are the 1 alt. type (most homogeneous layer order) and the Top/bottom type, which is a sandwich structure. In the case of the 1 alt. type failure was sudden and catastrophic in nature. As we increased the thickness of the matrix-only layers we moved towards more heterogeneous layer orders, the failure process changed, and delamination and matrix debonding became more prominent damage modes. The other extreme, which is the Top/bottom type (sandwich structure) inclined to produce the most ductile behavior with a multi-stage damage process. The results can be used to produce 3D-printed composite parts with predictable failure under bending load.

$$DI = -0.409 w_{matrix} + 1; \quad 0 < DI \leq 1 \tag{3}$$

where w_{matrix} (mm) is the thickness of the matrix-only layers.

Since the presence of voids is typical in 3D printed composites, the void content of the samples was also determined. Voids can promote crack propagation; therefore, they can influence the failure behavior too. We determined the total void content (Fig. 6/e) and the distribution of voids along the thickness of the specimen (*distance*) for a cross-section (Fig. 6/a-d). The void content was calculated as the ratio of voids to the total cross-section area. Total void content was the highest for the alt. 5, and the lowest for the Top/bottom type. The voids are present mostly in the reinforced layers, therefore the void distribution is analogous to the distribution of the reinforced layers in the specimens. The cross-sectional distribution of the voids may also explain the different failure behavior. In the case of a homogeneous distribution, crack propagation may be faster and thus elongation may be lower (alt. 1 and alt. 3 types). For more heterogeneous layer orders (alt. 5 and Top/bottom), crack propagation between the reinforced layers can be inhibited by the thicker matrix-only layers, which contain no voids.

3.2. Gradual failure behavior

The failure process shown in this study is very similar to the pseudo-ductile failure of resin matrix hybrid composites under tensile load [42–44]. Idarraga et al. [45] reported similar results for bending, and Huang and Joosten [22] achieved pseudo-ductile failure with 3D-printed hybrids. The novelty of our results is that 3D-printed composites can exhibit pseudo-ductile-like failure behavior under bending load, without hybridization, by the design of the layer order. Fig. 7 shows the 4 characteristic failure processes we found in the case of different layer orders. Table 1 summarises the corresponding mechanical responses. The quasi-linear stress-strain response (first and second cases) was observed for the alt. 1, alt. 1*, alt. 5, and the top/bottom types. The third case shows a more desirable, gradual failure, which was

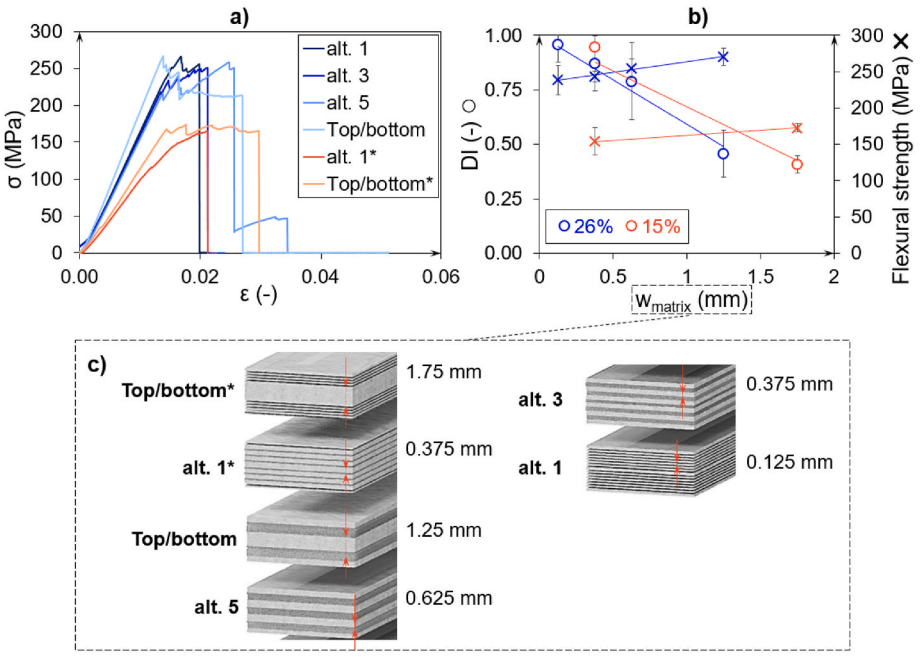

Fig. 5. a) Representative stress-strain curves for all layer orders, b) DI and the flexural strength as a function of the matrix layer thickness c) interpretation of the matrix layer thickness for all layer orders.

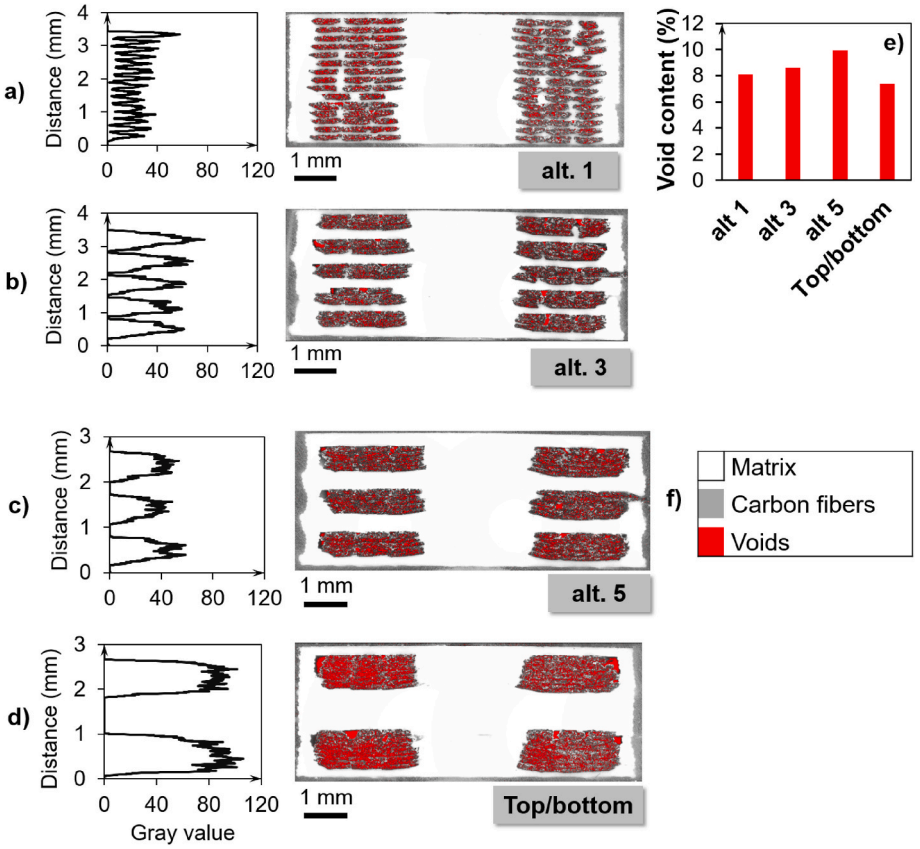

Fig. 6. Distribution of voids in a cross-section for the a) alt. 1, b) alt. 3, c) alt. 5, and d) Top/bottom types; g) the total void contents and f) shows the color legend for a)-d). (For interpretation of the references to color in this figure legend, the reader is referred to the Web version of this article.)

observed for the alt. 3 and the alt 1 types. The fourth case exhibits the maximum pseudo-ductile strain achievable for a given composite and, therefore can be considered ideal. This failure was specific to the top/-bottom* type. The first and the fourth mechanical responses were achieved only with lower (15 %) fiber content.

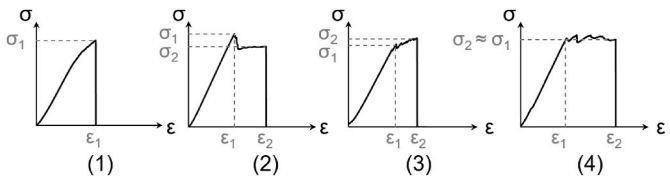

Fig. 7. Observed stress-strain responses under bending.

Table 1
Stress–strain response of the four damage scenarios.

No.	Region	Mechanical response
(1)	$0 < \sigma < \sigma_1$	Linear stress-strain response
	$\sigma = \sigma_1$	Catastrophic failure
(2)	$0 < \sigma < \sigma_1$	Linear stress-strain response until ε_1
	$\varepsilon_1 \leq \varepsilon < \varepsilon_2$	No stress increment until failure at $\sigma_2 < \sigma_1$
(3)	$\sigma < \sigma_1$	Linear stress-strain response until ε_1
	$\varepsilon_1 \leq \varepsilon < \varepsilon_2$	Non-linear stress-strain response until failure at $\sigma_2 > \sigma_1$
(4)	$0 < \sigma < \sigma_1$	Linear stress-strain response until ε_1
	$\varepsilon_1 \leq \varepsilon < \varepsilon_2$	Increase in strain until failure at $\sigma_2 \approx \sigma_1$

4. Conclusion

This research focuses on the flexural properties of 3D-printed continuous fiber–reinforced composites. Samples were prepared with a polyamide (PA) matrix and continuous carbon fiber (CF) reinforcement, and altogether six types of layer sequences were investigated, with two fiber volume fractions. The mechanical response for the flexural load was tested with 4-point bending experiments. We found that the layer order design greatly affects the failure behavior of the 3D-printed composites. We mapped the void distribution on the cross-sections and found that voids are mostly present in the reinforced layers. The void content ranged from 7.4 to 9.9 %. Samples with more homogeneous void distribution have lower toughness, which may be a consequence of faster crack propagation. The failure behavior ranges from catastrophic to pseudo-ductile, and four typical stress-strain responses can be distinguished. We found that a linear relationship can describe the effect of the thickness of unreinforced (matrix-only) layers on the ductility index, and toughness can be increased with increasing the thickness. In case of the most homogeneous layer order (for 26.3 % fiber content) the flexural strength and the ductility index were 238 ± 20 MPa and 0.96 (where 1 means completely brittle behavior), respectively. For the most heterogeneous layer order (sandwich structure) the flexural strength increased by 13.4 % while the ductility index decreased by 47.7 %, which corresponds to tougher behavior. Overall, our results show the failure process of 3D printed composites as a function of layer order, contributing to a more purposeful design and safer application.

CRediT authorship contribution statement

Csenge Tóth: Writing – original draft, Visualization, Validation, Methodology, Investigation, Conceptualization. **László Mihály Vas:** Writing – review & editing, Formal analysis. **Norbert Krisztián Kovács:** Writing – review & editing, Supervision, Resources, Project administration, Funding acquisition.

Declaration of competing interest

The authors declare that they have no known competing financial interests or personal relationships that could have appeared to influence the work reported in this paper.

Data availability

Data will be made available on request.

Acknowledgments

The research reported in this paper was supported by the National Research, Development and Innovation Office (NRDI, Hungary) through grants OTKA FK134336. Project no. TKP-6-6/PALY-2021 has been implemented with the support provided by the Ministry of Culture and Innovation of Hungary from the National Research, Development and Innovation Fund, financed under the TKP2021-NVA funding scheme. Csenge Tóth is thankful for the support of the ÚNKP-23-3-II-BME-140 New National Excellence Program of the Ministry for Culture and Innovation from the source of the National Research, Development and Innovation Fund. Supported by the ÚNKP-23-5-BME-466 New National Excellence Program of the Ministry for Culture and Innovation from the source of the National Research, Development and Innovation Fund and the János Bolyai Research Scholarship of the Hungarian Academy of Sciences.

References

[1] P. Cheng, Y. Peng, S. Li, Y. Rao, A. Le Duigou, K. Wang, S. Ahzi, 3D printed continuous fiber reinforced composite lightweight structures: a review and outlook, Compos. B Eng. 250 (2023), https://doi.org/10.1016/j.compositesb.2022.110450.
[2] X. Tian, A. Todoroki, T. Liu, L. Wu, Z. Hou, M. Ueda, Y. Hirano, R. Matsuzaki, K. Mizukami, K. Iizuka, A.V. Malakhov, A.N. Polilov, D. Li, B. Lu, 3D printing of continuous fiber reinforced polymer composites: development, application, and prospective, Chin. J. Mech. Eng.: Additive Manufacturing Frontiers 1 (2022) 100016, https://doi.org/10.1016/j.cjmeam.2022.100016.
[3] T.L.D.A. Montanheiro, V.M. Schatkoski, B.R.C. de Menezes, R.M. Pereira, R. G. Ribas, A. de S.M. de Freitas, A.P. Lemes, M.H.F.V. Fernandes, G.P. Thim, Recent progress on polymer scaffolds production: methods, main results, advantages and disadvantages, Express Polym. Lett. 16 (2022) 197–219, https://doi.org/10.3144/EXPRESSPOLYMLETT.2022.16.
[4] G. Kónya, P. Ficzere, The effect of layer thickness and orientation of the workpiece on the micro- and macrogeometric properties and the machining time of the part during 3D printing, Period. Polytech. - Mech. Eng. 67 (2023) 143–150, https://doi.org/10.3311/PPme.21473.
[5] A. Tessarin, M. Zaccariotto, U. Galvanetto, D. Stocchi, A multiscale numerical homogenization-based method for the prediction of elastic properties of components produced with the fused deposition modelling process, Results in Engineering 14 (2022) 100409, https://doi.org/10.1016/J.RINENG.2022.100409.
[6] E. Polyzos, D. Van Hemelrijck, L. Pyl, Stochastic modeling of the elastic response of parts produced by material extrusion using ideal voids, Int. J. Solid Struct. 279 (2023), https://doi.org/10.1016/j.ijsolstr.2023.112346.
[7] Q. He, H. Wang, K. Fu, L. Ye, 3D printed continuous CF/PA6 composites: effect of microscopic voids on mechanical performance, Compos. Sci. Technol. 191 (2020), https://doi.org/10.1016/j.compscitech.2020.108077.
[8] K. Saeed, A. McIlhagger, E. Harkin-Jones, C. McGarrigle, D. Dixon, M. Ali Shar, A. McMillan, E. Archer, Characterization of continuous carbon fibre reinforced 3D printed polymer composites with varying fibre volume fractions, Compos. Struct. 282 (2022), https://doi.org/10.1016/j.compstruct.2021.115033.
[9] K. Sugiyama, R. Matsuzaki, A.V. Malakhov, A.N. Polilov, M. Ueda, A. Todoroki, Y. Hirano, 3D printing of optimized composites with variable fiber volume fraction and stiffness using continuous fiber, Compos. Sci. Technol. 186 (2020), https://doi.org/10.1016/j.compscitech.2019.107905.
[10] S. Li, K. Wang, W. Zhu, Y. Peng, S. Ahzi, F. Chinesta, Investigation on the mechanical properties of 3D printed hybrid continuous fiber-filled composite considering influence of interfaces, Int. J. Adv. Manuf. Technol. 123 (2022) 3147–3158, https://doi.org/10.1007/s00170-022-10398-7.
[11] T. Liu, S. Yuan, Y. Wang, Y. Xiong, J. Zhu, L. Lu, Y. Tang, Stress-driven infill mapping for 3D-printed continuous fiber composite with tunable infill density and morphology, Addit. Manuf. 62 (2023), https://doi.org/10.1016/j.addma.2022.103374.
[12] Y. Huang, X. Tian, Z. Zheng, D. Li, A.V. Malakhov, A.N. Polilov, Multiscale concurrent design and 3D printing of continuous fiber reinforced thermoplastic composites with optimized fiber trajectory and topological structure, Compos. Struct. 285 (2022), https://doi.org/10.1016/j.compstruct.2022.115241.
[13] Y. Hu, R.B. Ladani, M. Brandt, Y. Li, A.P. Mouritz, Carbon fibre damage during 3D printing of polymer matrix laminates using the FDM process, Mater. Des. 205 (2021), https://doi.org/10.1016/j.matdes.2021.109679.
[14] J. Zhang, W. Yang, Y. Li, Process-dependent multiscale modeling for 3D printing of continuous fiber-reinforced composites, Addit. Manuf. 73 (2023), https://doi.org/10.1016/j.addma.2023.103680.
[15] P.F. Liu, J.Y. Zheng, Recent developments on damage modeling and finite element analysis for composite laminates: a review, Mater. Des. 31 (2010) 3825–3834, https://doi.org/10.1016/j.matdes.2010.03.031.
[16] G. Grail, S. Pimenta, S.T. Pinho, P. Robinson, Exploring the potential of interleaving to delay catastrophic failure in unidirectional composites under tensile loading, Compos. Sci. Technol. 106 (2015) 100–109, https://doi.org/10.1016/j.compscitech.2014.11.006.

[17] A. Alipour, R. Lin, K. Jayaraman, Enhancement of performance in flax/epoxy composites by developing interfacial adhesion using graphene oxide, Express Polym. Lett. 17 (2023) 471–486, https://doi.org/10.3144/expresspolymlett.2023.35.
[18] G.D. Goh, V. Dikshit, A.P. Nagalingam, G.L. Goh, S. Agarwala, S.L. Sing, J. Wei, W. Y. Yeong, Characterization of mechanical properties and fracture mode of additively manufactured carbon fiber and glass fiber reinforced thermoplastics, Mater. Des. 137 (2018) 79–89, https://doi.org/10.1016/j.matdes.2017.10.021.
[19] B. El Essawi, S. Abdallah, S. Ali, A. Nassir Abdo Mohammed, R.A. Susantyoko, S. Pervaiz, Optimization of infill density, fiber angle, carbon fiber layer position in 3D printed continuous carbon-fiber reinforced nylon composite, Results in Engineering (2024) 101926, https://doi.org/10.1016/j.rineng.2024.101926.
[20] B. Magyar, T. Czigany, G. Szebényi, Metal-alike polymer composites: the effect of inter-layer content on the pseudo-ductile behaviour of carbon fibre/epoxy resin materials, Compos. Sci. Technol. 215 (2021), https://doi.org/10.1016/j.compscitech.2021.109002.
[21] G. Szebényi, B. Magyar, T. Czigany, Achieving pseudo-ductile behavior of carbon fiber reinforced polymer composites via interfacial engineering, Adv. Eng. Mater. 23 (2021), https://doi.org/10.1002/adem.202000822.
[22] C. Huang, M.W. Joosten, 3D printed continuous fibre-reinforced composites: design and characterisation of advanced pseudo-ductile hybrid laminates, Compos Part A Appl Sci Manuf 146 (2021), https://doi.org/10.1016/j.compositesa.2021.106403.
[23] S. Vemuganti, E. Soliman, M.R. Taha, Exploiting fiber control for delayed failure in 3D printed fiber reinforced polymer composites, Compos. B Eng. 251 (2023), https://doi.org/10.1016/j.compositesb.2022.110495.
[24] S. Li, K. Wang, W. Zhu, Y. Peng, S. Ahzi, F. Chinesta, Contributions of interfaces on the mechanical behavior of 3D printed continuous fiber reinforced composites, Construct. Build. Mater. 340 (2022), https://doi.org/10.1016/j.conbuildmat.2022.127842.
[25] I. Fekete, F. Ronkay, L. Lendvai, Highly toughened blends of poly(lactic acid) (PLA) and natural rubber (NR) for FDM-based 3D printing applications: the effect of composition and infill pattern, Polym. Test. 99 (2021), https://doi.org/10.1016/j.polymertesting.2021.107205.
[26] Y. Peng, Y. Wu, S. Li, K. Wang, S. Yao, Z. Liu, H. Garmestani, Tailorable rigidity and energy-absorption capability of 3D printed continuous carbon fiber reinforced polyamide composites, Compos. Sci. Technol. 199 (2020), https://doi.org/10.1016/j.compscitech.2020.108337.
[27] H. Dou, W. Ye, D. Zhang, C. Wu, K. Huang, T. Sun, Y. Cheng, Three-point bending properties of 3D-printed continuous carbon fiber reinforced heterogeneous composites based on fiber content gradients, Adv. Eng. Mater. 25 (2023), https://doi.org/10.1002/adem.202200829.
[28] C. Zeng, L. Liu, W. Bian, Y. Liu, J. Leng, 4D printed electro-induced continuous carbon fiber reinforced shape memory polymer composites with excellent bending resistance, Compos. B Eng. 194 (2020), https://doi.org/10.1016/j.compositesb.2020.108034.
[29] F. Korkees, J. Allenby, P. Dorrington, 3D printing of composites: design parameters and flexural performance, Rapid Prototyp. J. 26 (2020) 699–706, https://doi.org/10.1108/RPJ-07-2019-0188.
[30] W.L.H. Wan A Hamid, L. Iannucci, P. Robinson, Flexural behaviour of 3D-printed carbon fibre composites: experimental and virtual tests - application to composite adaptive structure, Composites Part C: Open Access 10 (2023), https://doi.org/10.1016/j.jcomc.2022.100344.
[31] A.L. Amir, M.R. Ishak, N. Yidris, M.Y. Mohd Zuhri, M.R.M. Asyraf, M.R. Razman, Z. Ramli, Full-scale evaluation of creep coefficients and viscoelastic moduli in honeycomb sandwich pultruded GFRP composite cross-arms: experimental and numerical study, Results in Engineering (2024) 101850, https://doi.org/10.1016/j.rineng.2024.101850.
[32] T. Li, L. Wang, Bending behavior of sandwich composite structures with tunable 3D-printed core materials, Compos. Struct. 175 (2017) 46–57, https://doi.org/10.1016/j.compstruct.2017.05.001.
[33] S.Z. Mat Daud, J. Lim, M. Amir, S.W. Kim, Enhancing impact energy absorption in composite sandwich structures through synergistic smart material integration, Results in Engineering 21 (2024), https://doi.org/10.1016/j.rineng.2024.101902.
[34] C. Zeng, L. Liu, W. Bian, J. Leng, Y. Liu, Bending performance and failure behavior of 3D printed continuous fiber reinforced composite corrugated sandwich structures with shape memory capability, Compos. Struct. 262 (2021), https://doi.org/10.1016/j.compstruct.2021.113626.
[35] Z. bo Pan, W. Zhou, K. Zhang, L. hua Ma, J. Liu, Flexural damage and failure behavior of 3D printed continuous fiber composites by complementary nondestructive testing technology, Polym. Compos. 43 (2022) 2864–2877, https://doi.org/10.1002/pc.26582.
[36] N. Maqsood, M. Rimašauskas, Tensile and flexural response of 3D printed solid and porous CCFRPC structures and fracture interface study using image processing technique, J. Mater. Res. Technol. 14 (2021) 731–742, https://doi.org/10.1016/j.jmrt.2021.06.095.
[37] A.R. Prajapati, H.K. Dave, H.K. Raval, An experimental study on mechanical, thermal and flame-retardant properties of 3D-printed glass-fiber-reinforced polymer composites, J. Mater. Eng. Perform. 30 (2021) 5266–5277, https://doi.org/10.1007/s11665-021-05731-2.
[38] Markforged material datasheet, (https://web-objects.markforged.com/craft/materials/CompositesV5.2.pdf) (Accessed 13 March 2024).
[39] Y. Yin, Y. Qiao, S. Hu, Four-point bending tests for the fracture properties of concrete, Eng. Fract. Mech. 211 (2019) 371–381, https://doi.org/10.1016/j.engfracmech.2019.03.004.
[40] J. Karger-Kocsis, Instrumented impact fracture and related failure behavior in short-and long-glass-fiber-reinforced polypropylene, Compos. Sci. Technol. 48 (1993), https://doi.org/10.1016/0266-3538(93)90144-6.
[41] L. Li, W. Liu, L. Sun, Mechanical characterization of 3D printed continuous carbon fiber reinforced thermoplastic composites, Compos. Sci. Technol. 227 (2022), https://doi.org/10.1016/j.compscitech.2022.109618.
[42] M. Jalalvand, G. Czél, M.R. Wisnom, Damage analysis of pseudo-ductile thin-ply UD hybrid composites - a new analytical method, Compos Part A Appl Sci Manuf 69 (2015) 83–93, https://doi.org/10.1016/j.compositesa.2014.11.006.
[43] G. Czél, M. Jalalvand, M.R. Wisnom, T. Czigány, Design and characterisation of high performance, pseudo-ductile all-carbon/epoxy unidirectional hybrid composites, Compos. B Eng. 111 (2017) 348–356, https://doi.org/10.1016/j.compositesb.2016.11.049.
[44] S.B. Sapozhnikov, Y. Swolfs, S.V. Lomov, Pseudo-ductile unidirectional high modulus/high strength carbon fibre hybrids using conventional ply thickness prepregs, Compos. B Eng. 198 (2020), https://doi.org/10.1016/j.compositesb.2020.108213.
[45] G. Idarraga, M. Jalalvand, M. Fotouhi, J. Meza, M.R. Wisnom, Gradual failure in high-performance unidirectional thin-ply carbon/glass hybrid composites under bending, Compos. Struct. 271 (2021), https://doi.org/10.1016/j.compstruct.2021.114128.